Int. Jr. of Engineering, Contemporary Mathematics and Sciences
Vol. 1, No. 1, January-June 2015

ISSN No: 2250-3099

Adaptative mesh in boundary elements method for the calculation of hydrodynamic interactions in creeping flow

Lassaad El Asmi, Maher Berzig and François Feuillebois

Laboratoire d'Ingénierie Mathématique, Ecole polytechnique de Tunisie, BP 743, 2078 la Marsa Tunisie

assaad.elasmi@ept.rnu.tn

Université de Tunis, Ecole Supérieure des Sciences et Techniques de Tunis

maher.berzig@gmail.com

LIMSI-CNRS, Université de Paris-Sud, 91403 ORSAY, France

Francois.Feuillebois@limsi.fr

Abstract. The hydrodynamic interactions between particles in the vicinity of a wall in creeping flow are calculated with the boundary elements method. The mesh refinement technique proposed here is adapting to large local stress gradients. It is appropriate to describe hydrodynamic interactions in complex geometries and in particular in lubrication regions. Results are validated against classical results for a sphere and wall. As examples of application, flow trajectories are presented for various configurations involving one or several spheres and prolate spheroids either held fixed in a shear flow or moving in a fluid at rest in the vicinity of a plane wall.

Keywords: Creeping flow, Boundary integral method, Adaptative mesh.
2000 Mathematics Subject Classification: 76M20, 65M06, 76D07.

1 Introduction

The problem of solid particles in the flow of a viscous fluid along a solid plane wall is considered here. The Reynolds number is assumed to be low and the creeping flow equations to apply. The flow field is obtained with the classical boundary element method (see e.g. [6]). There has been various ways to mesh particles for this problem (see e.g. [7]). Here, interactions between particles and the wall at the scale of particles are refined by using a novel adaptative mesh technique based on the intensity of the local surface stress.

The solution for several translating and rotating particles in a shear flow along a wall is obtained as the sum of elementary problems: (i) each particle in turn is either translating or rotating and the other particles are fixed in a fluid at rest; (ii) all particles are fixed in an ambient shear flow. Our peculiar adaptative mesh technique is well adapted to take into account the multiple hydrodynamic interactions in these complex geometries.

The boundary element method integral equation is recalled in section 2. Our adaptative mesh then is presented in section 3. Finally results are presented in section 5.

2 Boundary element method integral equation

The classical integral formulation (2.1) provides a duality relationship between the fluid velocity $\mathbf{v}$ at a point $\mathbf{x}$ and the stress $\mathbf{q}$ at a point $\mathbf{y}$ on the spheres surface S:

$$\mathbf{v}(\mathbf{x}) = \int_S \mathbf{G}(\mathbf{x}, \mathbf{y})\,\mathbf{q}(\mathbf{y})\, dS_{\mathbf{y}} \qquad \mathbf{x} \in S \tag{2.1}$$

The problem consists in finding the stress when the fluid velocity is prescribed on surfaces. The fluid velocity then is obtained at any point $\mathbf{x}$ in the fluid domain using the same formula (2.1). The force and torque on each sphere are obtained from the calculated stresses on that sphere. Since solid particles are considered here, the kernel only consists of a single layer potential which appears as the Green function $\mathbf{G}$. That is, the double layer potential vanishes ([9]).

The no-slip on the plane wall is accounted for by using the Green function $\mathbf{G}$ calculated by [1] for a Stokeslet in the vicinity of a wall, as was done e.g. by [8].

Eq.(2.1) is discretized by constructing N_t triangles on each of the N_p particles and applying the boundary condition for the fluid velocity at the center of each triangle. Since the velocity has three components, this provides thus a linear system of $3 \times n_p \times N_t$ equations for the unknown stresses. Thus, the three components of the stress may be obtained at the center of each triangle. The way to construct the triangles is explained in the next section.

3 Adaptative mesh depending on local stress

At the first level of refinement, the particles surfaces are first meshed starting with an octahedron, as in [6].

The next refinement levels consist classically in dividing each triangle into four elementary triangles. Thus at the r^{th} refinement level, there are $N_t = 8 \times 4^r$ triangles on each particle. A drawback is that the size of the algebraic system to be solved may then become unnecessary large and its condition number may also increase.

A local refinement technique is therefore proposed here. Starting from a given refinement level, the sequence for refining the mesh consists first in calculating the stresses on each triangular element. Triangles then are distributed in classes depending on the value of the stress. Triangles then are renumbered depending on their class of stress, as schematically shown in Fig. 1.

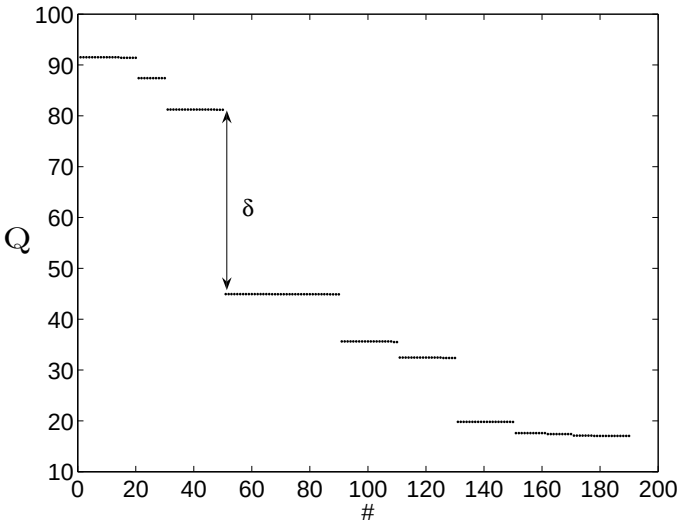

Figure 1 Values of the stress in the various classes, versus the triangle number (after renumbering).

From this ordering, areas with the highest gradient of surface stresses are selected as regions where triangles have to be divided into four elementary triangles. Typically, the three largest values of δ are selected (see Fig. 1) and the triangles of the corresponding classes are refined. This process may be repeated to decrease the values of the δ's.

This scheme may be repeated, starting from the preceding level of refinement, as many times as necessary to a achieve a prescribed tolerance.

As an example, the mesh refinement due to wall effect is presented for a single sphere located at various distances from a wall in Fig. 2. When the sphere is closer to the wall, the stresses are larger because of lubrication and therefore the mesh is refined accordingly.

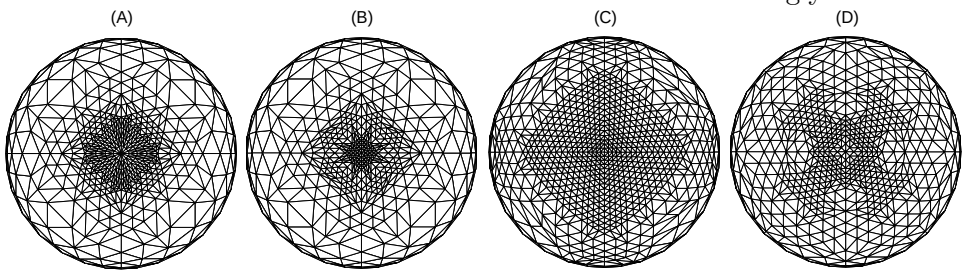

Figure 2 Mesh refinement of a sphere in the region of high stresses, for dimensionless gaps of 0.001 (A), 0.006 (B), 0.02 (C), 0.1 (D).

Results for the drag force obtained with a standard mesh at levels 2, 3 and an adaptative mesh starting from level 2 are compared with the exact results of [10] in Fig. 3. The force is here normalized by the Stokes drag force on a sphere translating with the same velocity in unbounded fluid. It is plotted versus the dimensionless gap $L-1$, where L denotes the sphere center to wall distance normalized by the sphere radius. The advantage of our adaptative mesh is made clear here, since our solution is closer to the exact formula for small gaps $L-1$, a situation when lubrication results in large stress gradients.

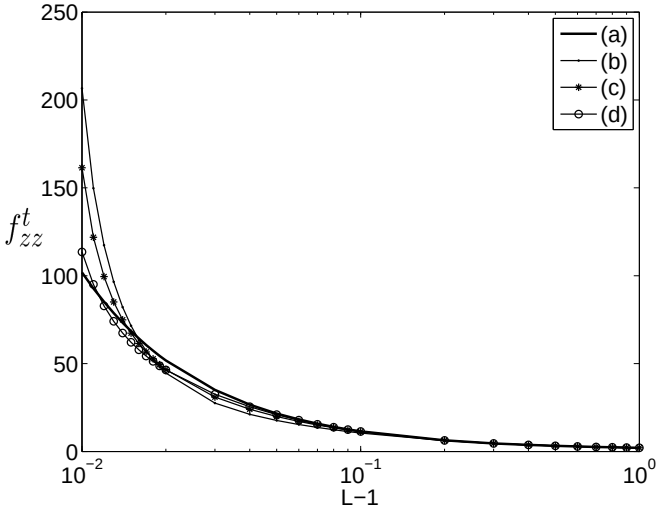

Figure 3 Normalized drag force f^t_{zz} on a sphere settling towards a plane versus the dimensionless gap $L-1$. The exact solution of [10] (a) is compared with the BEM solution using: (b) an uniform mesh at level 2; (c) an uniform mesh at level 3; (d) an adaptative mesh starting from the uniform mesh at level 2.

4 Validation

The technique is further validated by considering asymmetrical flows for a sphere close to a wall. Our BEM results are compared with the exact results obtained by [11] using the bispherical coordinates technique (BIS). The notation here is like in that paper. Let a be the sphere radius. Consider a rectangular system (x, y, z), the wall being at $z = 0$.

For a sphere translating with velocity U_x along the wall (say along x) in a fluid at rest, the drag force F^t_x is along x and there is also a torque along y:

$$\begin{aligned} F^t_x &= -6\pi a\mu f^t_{xx} U_x \\ C^t_y &= 8\pi a^2 \mu\, c^t_{yx} U_x \end{aligned}$$

The superscript (t) denotes translation. In the friction factors f, c, the first subscript denotes the direction of the force or torque and the second subscript denotes the direction of the motion. The results for the friction factors are displayed in Figs. 4. The abscissa $L-1$ in these figures denotes the dimensionless gap between the sphere and the wall, $L = \ell/a$ being the distance between the sphere center and wall.

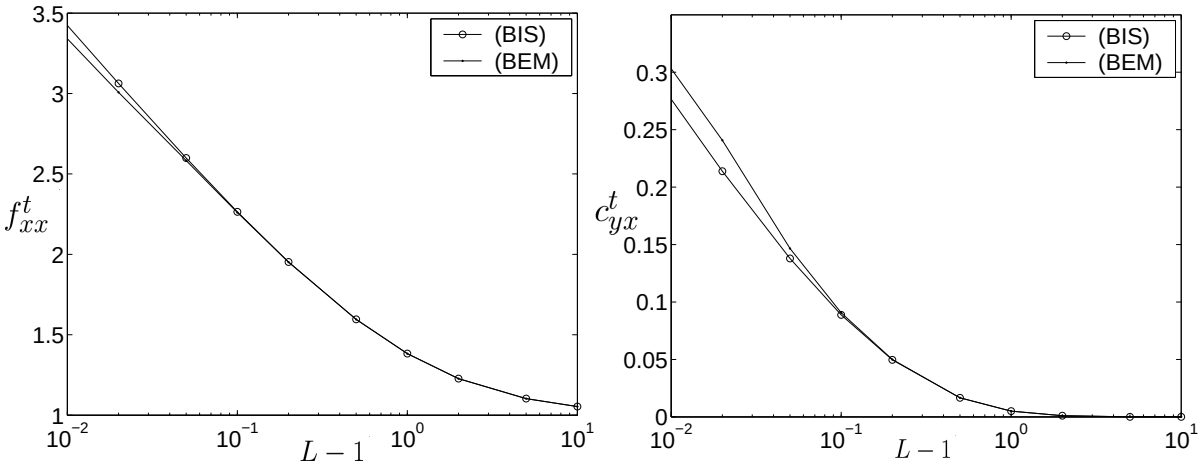

Figure 4 Normalized drag (left) and torque (right) on a sphere translating along a wall versus the dimensionless gap $Z-1$ between the sphere and the wall. Our results using BEM and exact results using BIS.

A sphere rotating along y with a velocity Ω_y is submitted to a torque along y and also to a force along x:

$$\begin{aligned} C^r_y &= -8\pi a^3 \mu\, c^r_{yy} \Omega_y \\ F^r_x &= 6\pi a^2 \mu f^r_{xy} \Omega_y \end{aligned}$$

The superscript (r) denotes rotation. The results for the friction factors are in Figs. 5.

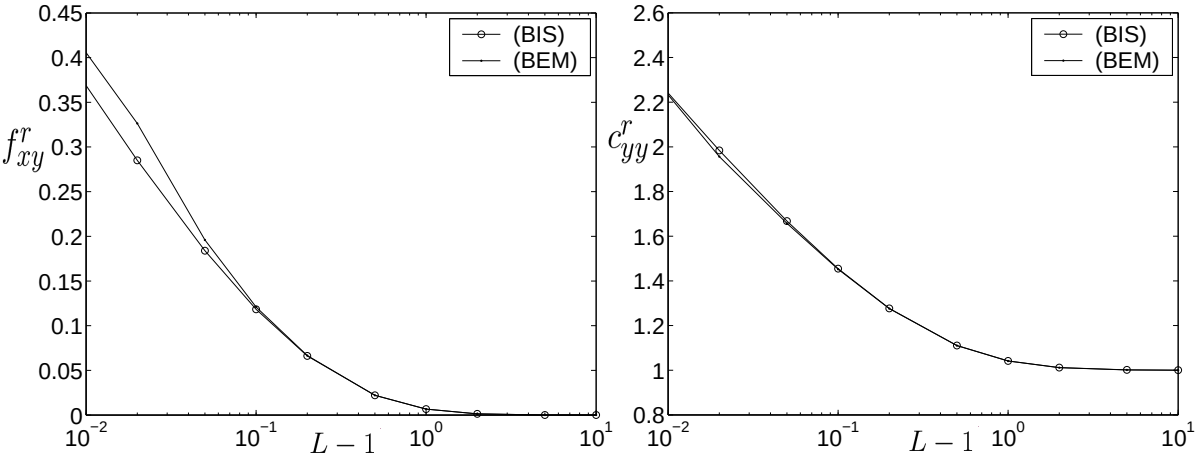

Figure 5 Same as in Fig.4 but for a sphere rotating along an axis parallel to the wall.

Consider then a sphere held fixed in a shear flow with velocity

$$v^\infty = \kappa z\, \mathbf{e}^1 \tag{4.1}$$

where κ is the shear rate and $\mathbf{e}^1$ is the unit vector along x. There are a force and a torque on the sphere:

$$\begin{aligned} F^\kappa_x &= 6\pi a \mu f^\kappa_{xx} \kappa \ell \\ C^\kappa_y &= 4\pi a^3 \mu c^\kappa_{yx} \kappa \end{aligned}$$

The superscript (κ) denotes the shear flow. Results for the friction factors are in Fig. 6.

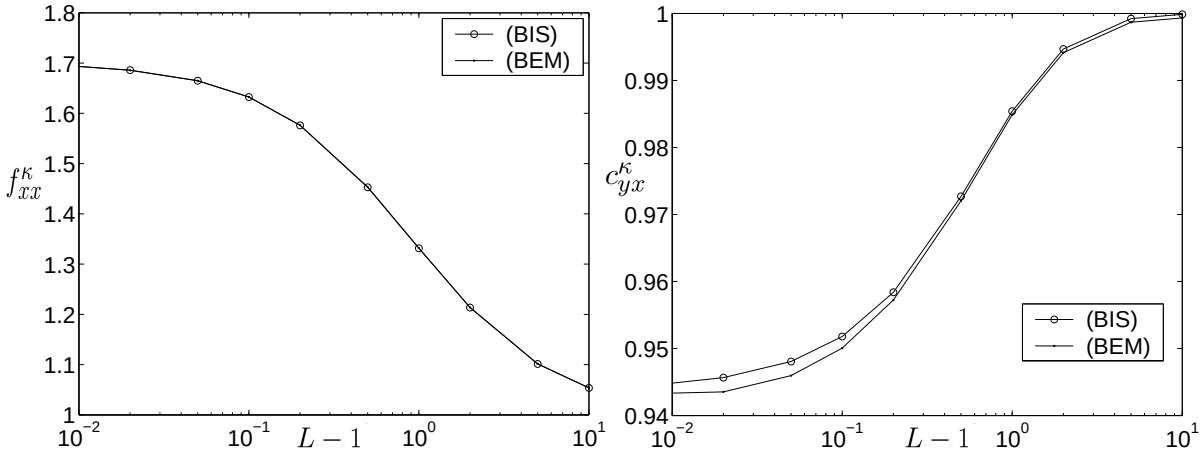

Figure 6 Same as in Fig. 4 but for a sphere held fixed in a shear flow along a wall.

5 Results

This technique is well adapted to treat any number of particles and complex geometries.

5.1 Fluid trajectories around spherical particles

Some typical examples are presented for the fluid trajectories around spherical particles. Two equal spheres are considered in Fig. 7 and 8 and three equal spheres in Fig. 9 and 10.

In Fig. 7, two equal spheres are fixed in a shear flow defined in Eq. (4.1). In configuration (A) the line of centers is parallel to the wall; spheres are centered at positions (normalized with their radius) $(0, -3, 3)$ and $(0, 3, 3)$. In configuration (B), it is normal to the wall, spheres being centered at $(0,\ 0,\ 3)$ and $(0,\ 0,\ 6)$.

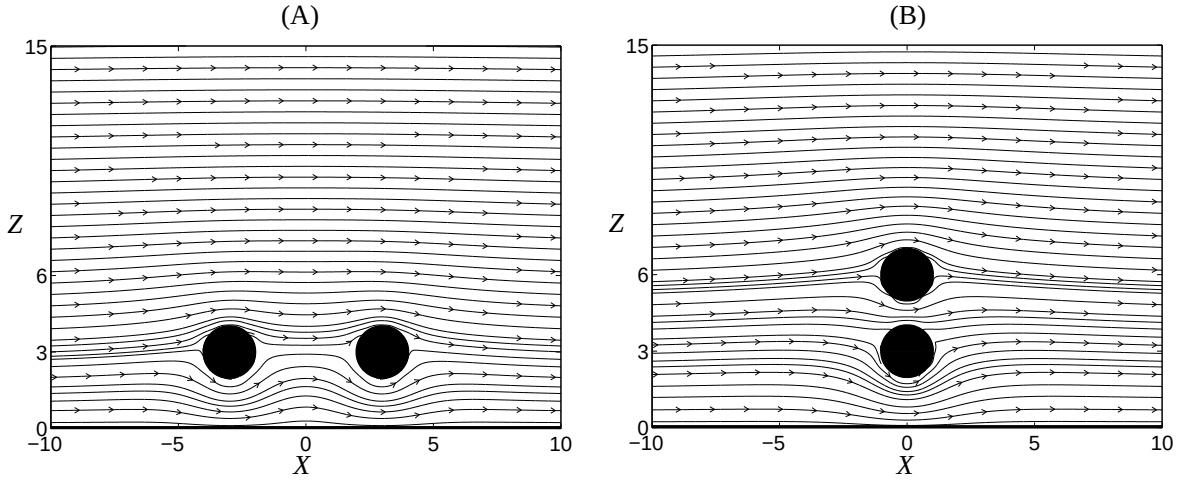

Figure 7 Fluid trajectories around two equal spherical particles fixed in a shear flow parallel to the wall.

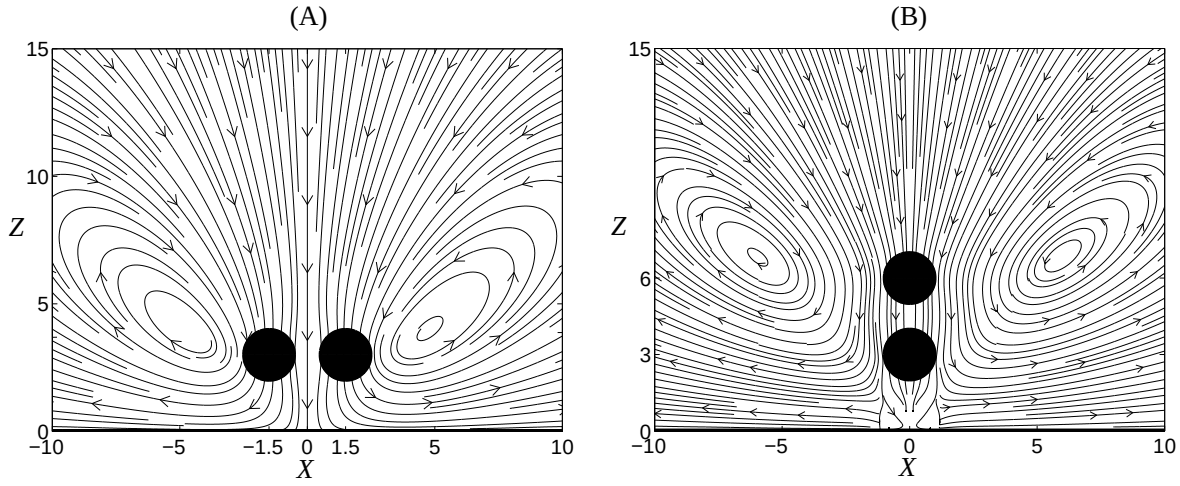

Figure 8 Fluid trajectories around two equal spherical particles moving with equal velocities in the direction normal to the wall.

In Fig. 8, two equal spheres are moving normal to the wall with equal velocities in a fluid at rest. In configuration (A) spheres are centered at positions (normalized with their radius) $(0, -1.5, 3)$ and $(0, 1.5, 3)$. In configuration (B), they are centered at (0, 0, 3) and (0, 0, 6). For these flow fields, it is observed that the Stokeslets inside the particle create large recirculating regions.

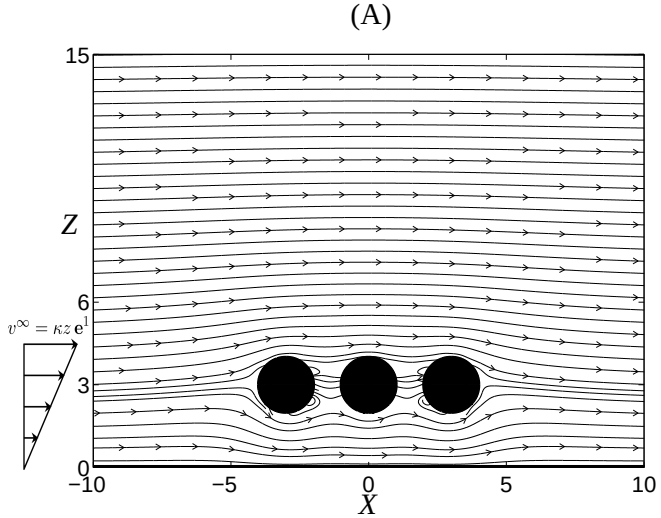

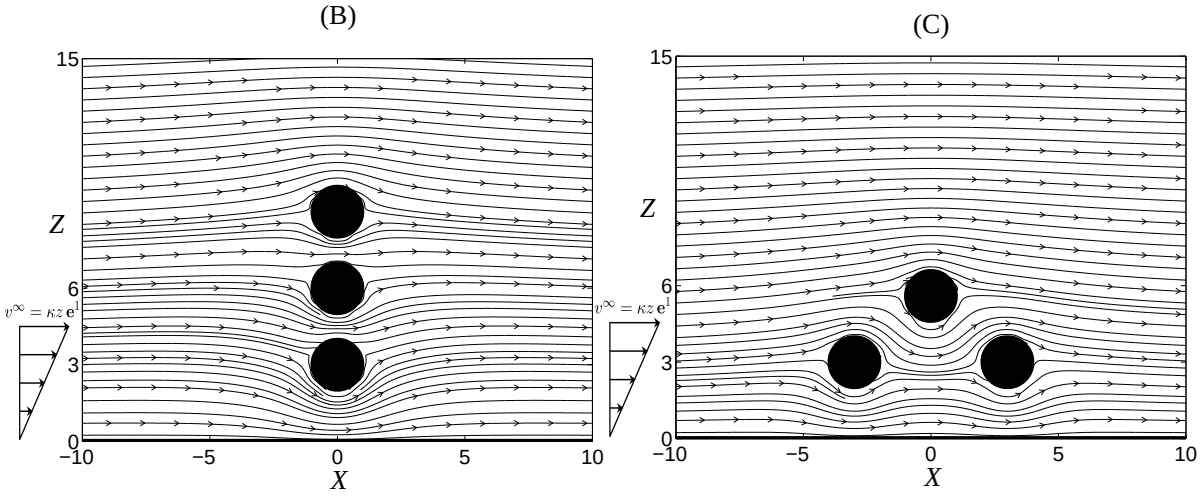

Figure 9 Fluid trajectories around three particles fixed in a shear flow. The centers of the spheres are: (A) aligned parallel to the wall; (B) aligned normal to the wall; (C) on a the summits of a triangle. The coordinates of sphere centers are given in the text.

Fig. 9 shows the fluid trajectories around three spherical particles fixed in a shear flow defined in Eq. (4.1). The spheres centers are located in the (x, z) plane. In configuration (A) the line of centers is parallel to the wall, the centers being at $(0, -3, 3), (0, 0, 3), (0, 3, 3)$, in configuration (B), it is normal to the wall the centers being at $(0, 0, 3), (0, 0, 6), (0, 3, 9)$ and in configuration (C) spheres are centered at the summits of a triangle, the centers being at $(0, -1.5, 3), (0, 0, 3(1 + \sqrt{3}/2)), (0, 1.5, 3)$

Fig. 10 shows fluid trajectories around three spherical particles moving normally to a wall with the same velocity. The configurations are the same as in Fig. 9.

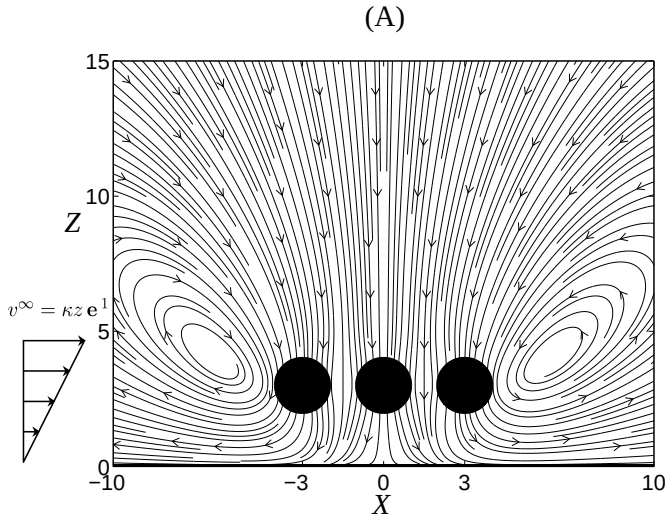

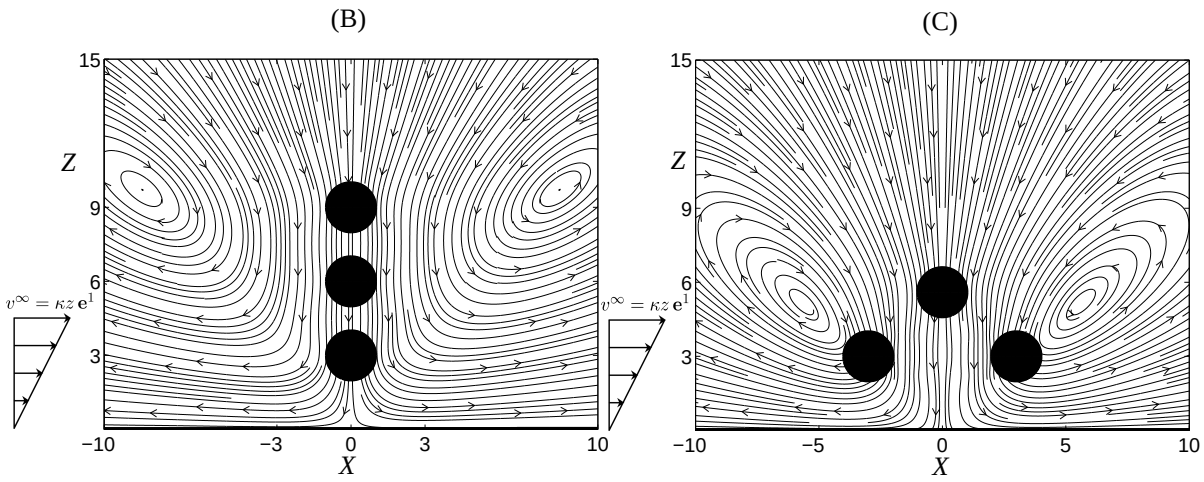

Figure 10 Fluid trajectories around three spherical particles moving normally to a wall with identical velocities. Same configurations as in Fig. 9.

For all these cases, values of the normalized forces acting on the spheres were calculated and are available from the authors on request.

5.2 A prolate spheroid in a shear flow near a wall

Consider a prolate spheroid held fixed in a shear flow defined in Eq. (4.1), the wall being as above at $z = 0$.

The case of a spheroid far from the wall is considered first. The particle symmetry axis is located in the plane of the shear flow (the (x, z) plane), and is along the $x = z$ line. Our results for the components of the drag along the x and z axes are presented in table 5.2 for various values of the ratio a/c of the semi-minor to the semi-major axes. They are compared with the results of [12] for the same configuration and with the results of [13] for the limit case of a spheroid in unbounded fluid. All results are in good agreement. Note that in our case, less than 512 triangles were used whereas [12] used 1200 triangles.

	$F_x^\kappa/\mu c\kappa z$		
a/c	(a)	(b)	(c)
0.1	6.088	6.055	6.104
0.2	7.834	7.798	7.841
0.35	10.079	10.027	10.081
0.5	12.172	12.105	12.171
0.7	14.872	14.789	14.870
0.8	16.204	16.113	16.201
0.9	17.529	17.432	17.527
0.95	18.190	18.089	18.188
0.990	18.718	18.614	18.716
0.9999	18.848	18.744	18.846
0.999999	18.850	18.747	18.848

	$F_z^\kappa/\mu c\kappa z$		
a/c	(a)	(b)	(c)
0.1	-1.098	-1.088	-1.109
0.2	-1.105	-1.106	-1.112
0.35	-0.999	-1.002	-1.004
0.5	-0.825	-0.827	-0.827
0.7	-0.529	-0.530	-0.529
0.8	-0.362	-0.363	-0.362
0.9	-0.185	-0.186	-0.185
0.95	-0.094	-0.095	-0.093
0.990	-0.019	-0.021	-0.019
0.9999	-0.000	-0.002	-0.000
0.999999	-0.000	-0.000	-0.000

Table 1 A prolate spheroid far from the wall $z = 0$ in a shear flow with velocity $\mathbf{v}^\infty = \kappa z\, \mathbf{e}^1$. Dimensionless drag force along x (top) and along z (bottom). (a) Analytical results of [13] for a sphere in an unbounded shear flow, (b) results of [12] (c) our results.

5.3 A prolate spheroid moving perpendicularly to a wall

Consider a prolate spheroid with $a/c = 1/3$ moving perpendicularly to a wall in a fluid at rest. The semi-major axis (with dimension c) is parallel to the wall. The drag force on the spheroid is normalized with the drag on a sphere of the same volume, that is the volume $\frac{4}{3}\pi a^2 c$, when moving in unbounded fluid. Results for the dimensionless drag force are presented in Fig. 11 versus the dimensionless gap ($L-1$ after normalizing by a) between the spheroid and the wall. They are compared with those for the sphere of the same volume.

It is observed that because of the flatness of the spheroid in the near wall region, the drag is much larger than that on the sphere. Our meshing technique is well adapted to describe this situation.

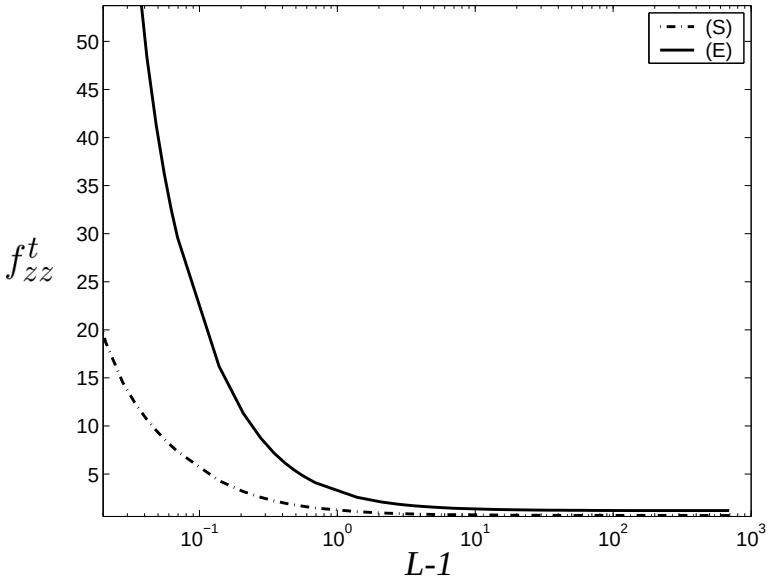

Figure 11 Normalized force exerted on a prolate spheroid moving perpendicularly to a wall (E) compared with the normalized drag on a sphere (S) with the same center and same volume.

5.4 Interaction between two prolate spheroids near a wall

Consider now two identical prolate spheroids with $a/c = 1/3$ moving near a wall $z = 0$ in a fluid at rest. Lengths are normalized by a. In a dimensionless coordinate system (X, Y, Z), the equations of the two spheroids are:

$$(X \pm 3)^2 + \frac{Y^2}{9} + (Z - L)^2 = 1$$

As above, the drag forces on the spheroids are normalized with the drag on a sphere of the same volume when moving in unbounded fluid. Results for the dimensionless drag forces are shown in table 2 for the cases when the spheroids are both translating normally to the wall (F^t_{zz}) and along the wall in the direction of their semi-major axis (F^t_{yy}).

	f^t_{zz}		f^t_{yy}	
$L-1$	(1)	(2)	(1)	(2)
0.01	114.58	114.58	2.280	2.280
0.02	30.866	30.866	1.977	1.977
0.04	14.644	14.644	1.763	1.763
0.06	10.653	10.653	1.641	1.641
0.08	8.602	8.602	1.555	1.555
0.1	7.280	7.280	1.487	1.487
0.5	2.233	2.233	1.023	1.023
1	1.498	1.498	0.864	0.864
5	0.857	0.857	0.646	0.646
10	0.742	0.742	0.606	0.606
50	0.640	0.640	0.568	0.568

Table 2 Normalized drag forces on two spheroids moving with the same velocity in a fluid at rest, normally to a wall (left) and parallel to a wall (right).

6 Fluid trajectories around spheroidal particles

Fluid trajectories around equal prolate spheroids with the same aspect ratio as above are presented in Fig. 12. The particles are held fixed in a shear flow.

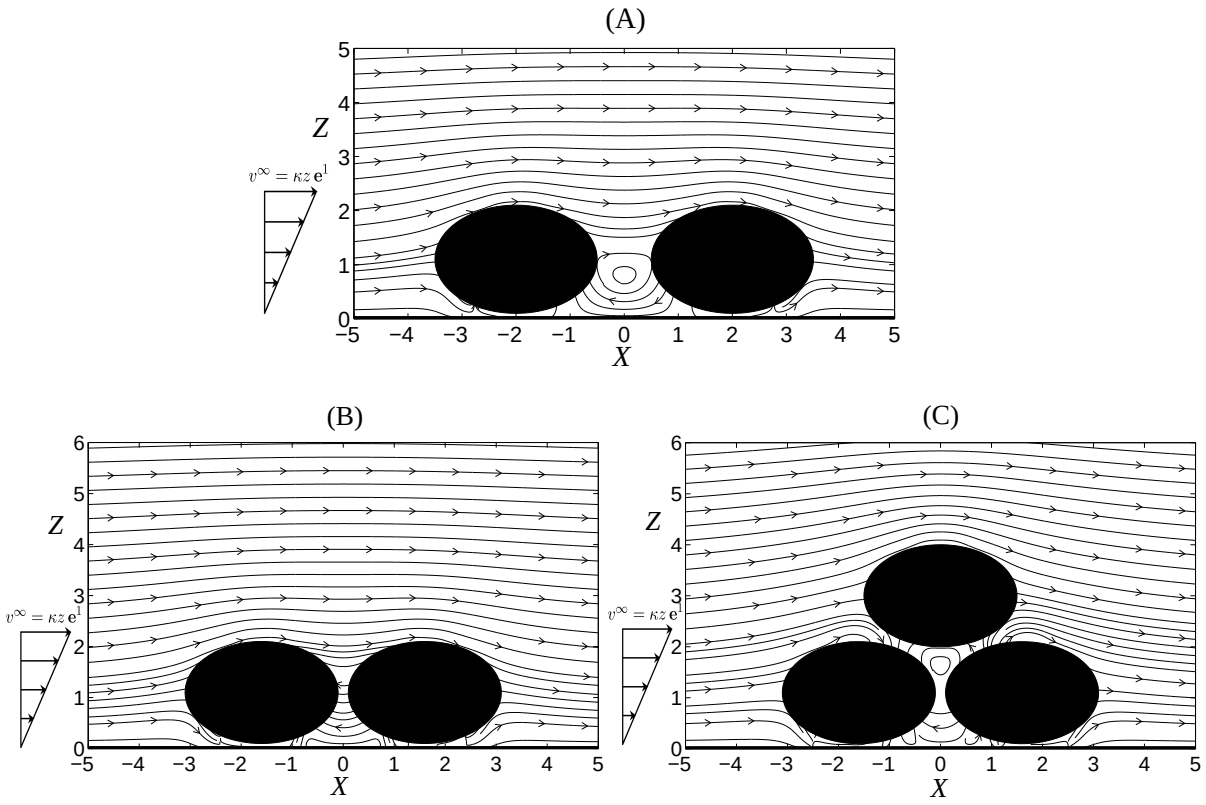

Figure 12 Fluid trajectories around spheroidal particles fixed in a shear flow: two particles with centers at $(-2, 0, 1.1)$ and $(2, 0, 1.1)$ for (A); $(-1.6, 0, 1.1)$ and $(1.6, 0, 1.1)$ for (B); three particles centered at $(-1.6, 0, 1.1), (1.6, 0, 1.1), (0, 0, 3)$ for (C).

7 Conclusions

The BEM technique is applied with a mesh refinement consisting in dividing triangles in the areas of large stress gradient. This technique is appropriate for configurations where lubrication effects are important. The results of the technique are compared to various earlier results for validation. As examples of application, flow trajectories are presented for various configurations involving one or several spheres and prolate spheroids, the particles being either fixed in a shear flow near a wall or moving normally to the wall in a fluid at rest.

References

[1] J.R. Blake, A note on the image system for a stokeslet in a no-slip boundary, Proc. Camb. Phil. Soc. 70 (1971) 303–310.

[2] L. Elasmi, M. Berzig and F. Feuillebois, Stokes flow for the axisymmetric motion of several spherical particles perpendicular to a plane wall, ZAMP. 54 (2003) 304-327.

[3] C. Pozrikidis, Boundary integral and singularity method for linearized viscous flow, Cambridge University Press. (1992).

[4] C. Pozrikidis, Numerical Computation in Science and Engineering, Oxford University Press. (1998).

[5] C. Pozrikidis, Fluid Dynamics, Theory, Computation, and Numerical Solution, Kluwer Academic Publishers. (2001).

[6] C. Pozrikidis, A Practical Guide to Boundary Element Methods with the Software Library Bemlib, CRC Press. (2002).

[7] M. Loewenberg and E.J. Hinch, Numerical simulation of a concentrated emulsion in shear flow, J. Fluid Mech. 321 (1996) 395-419.

[8] A. Sellier, Settling motion of interacting solid particles in the vicinity of a plane solid boundary, C. R. Mécanique. 333 (2005)413-418.

[9] O.A. Ladyzhenskaya, Mathematical theory of viscous incompressible flow, Gordon and Breach. (1969).

[10] H. Brenner, The slow motion of a sphere through a viscous fluid towards a plane surface, Chem. Eng. Sci. 16 (1961)242-251.

[11] M. Chaoui and F. Feuillebois, Creeping flow around a sphere in a shear flow close to a wall, Q. J. Mech. Appl. Math. 56 (2003) 231-410.

[12] E. Gavze and M. Shapiro, Particles in a shear flow near a solid wall: effect of nonsphericity on forces and velocities, Int. J. Multiphase Flow. 23 (1997)155-182.

[13] G.B. Jeffery, The motion of ellipsoidal particles immersed in a viscous fluid, Proc. Roy. Soc. London. Series A. 102 (1922) 161-179.